Chinese Chemical Letters 33 (2022) 3681–3694

Contents lists available at ScienceDirect

Chinese Chemical Letters

journal homepage: www.elsevier.com/locate/cclet

Synthesis of 3D printing materials and their electrochemical applications

Huijie Zhou, Hui Yang, Shiyi Yao, Li Jiang, Nuochen Sun, Huan Pang*

School of Chemistry and Chemical Engineering, Yangzhou University, Yangzhou 225009, China

ARTICLE INFO

Article history:
Received 15 September 2021
Revised 22 October 2021
Accepted 2 November 2021
Available online 11 November 2021

Keywords:
3D printing
Micro/nano materials
Supercapacitors
Batteries
Electrocatalysis

ABSTRACT

Three-dimensional (3D) printing, also known as additive manufacturing, has the advantages of low cost, easy structure operation, rapid prototyping, and easy customization. In the past few years, materials with different structures, compositions, and properties have been widely studied as prospects in the field of 3D printing. This paper reviews the synthesis methods and morphologies of one-, two- and three-dimensional micro/nano materials and their composites, as well as their applications in electrochemistry, such as supercapacitors, batteries and electrocatalysis. The latest progress and breakthroughs in the synthesis and application of different structural materials in 3D-printing materials, as well as the challenges and prospects of electrochemical applications, are discussed.

1. Introduction

With the continuous improvement in social living standards and technology, traditional electronic equipment cannot meet contemporary needs [1–8]. Therefore, the use of advanced manufacturing technology to customize electrode structure is a key method in improving the electrochemical properties of electrode materials [9–17]. Three-dimensional (3D) printing, also called additive manufacturing, is a technical means of computer-aided design and forming [18–27]. Unlike traditional manufacturing, 3D printing is highly flexible. However, the preparation and processing of ink and raw materials is a key factor in 3D structure design, particularly for 3D direct ink writing [28–35]. The ink required for 3D printing is usually applied through colloid, suspension/dissolution polymer, or electrolyte block to liquid, and flow performance is achieved by design adjustment. In the printing process, a low viscosity ink forms droplets and deposits easily, while a high viscosity ink forms a continuous rod flame [30,36–42]. Choosing the right material to modulate the ink with shear thinning characteristics is the key in meeting printing requirements. Therefore, in order to make 3D printing feasible, printable inks must have high viscosity and specific rheological properties (shear thinning) to achieve high resolution and rapid prototyping. Thus, selecting appropriate materials to adjust the ink with desired shear dilution characteristics is a key point to achevie the printing requirements. The structure and electronic properties of materials play a critical role in the mechanical and electrochemical properties of materials. The morphology and properties of the materials is largely influenced by different synthesis schemes. In addition, the mechanical properties of materials can be changed to a certain extent by adding various additives and regulating the morphology of materials [30,43–48]. In addition, during ink deposition and curing, the ink is required to have a certain degree of mechanical strength and stiffness to support the entire electrode structure. To achieve a stable dispersion, promote the transformation of fluid to gel, ensure the retention of printing shape, and fully integrate with the first precipitating base, it is necessary to control and adjust the rheological properties of ink formulations and materials.

Nowadays, 3D printing has been widely used to construct a variety of electrode structures, but its electrochemical performance is relatively poor due to the slow diffusion kinetics of ions and electrons. However, with the rapid development of nanotechnology, various functional nanomaterials can be applied to 3D printing and engineering fields to make up for their shortcomings [49–52]. Nanomaterials with a relatively large specific surface area have the advantage of convenient ion migration; therefore, they have significant advantages in electrochemical applications [50,53,54]. When a 3D-printed electrode contains nanomaterials, the electrochemical activity of the material considerably increases [45,55,56]. In 3D printing, it is difficult to print accurately on several nano- or sub-nanoscales. However, in printing technology, postprocessing and embedding chemical methods can effectively eliminate these limitations through the preparation of hydrogel ink, the construction of soft and hard templates, and the synthesis of porous ma-

* Corresponding author.
E-mail address: panghuan@yzu.edu.cn (H. Pang).

https://doi.org/10.1016/j.cclet.2021.11.018
1001-8417/

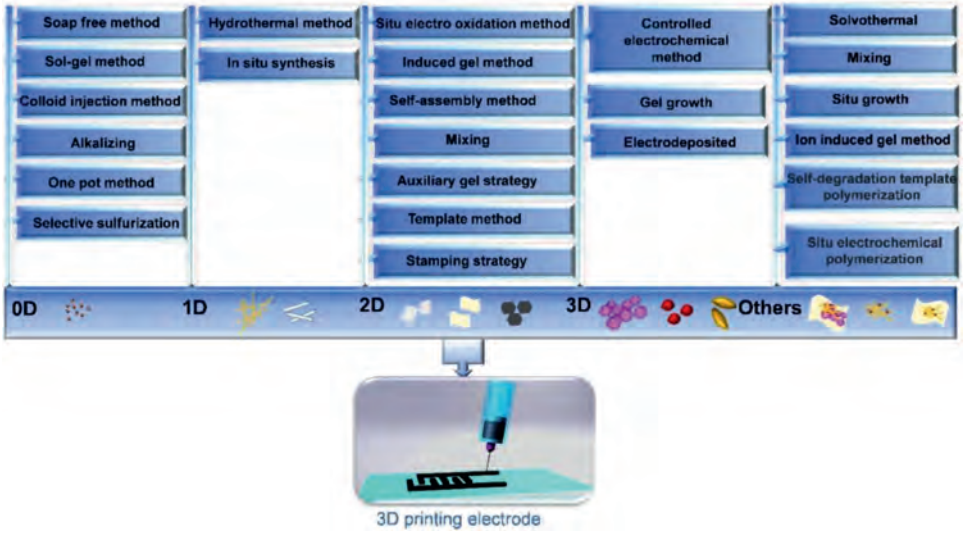

Fig. 1. Summary of common synthetic approaches for 3D printing materials with different morphologies.

terials. With the rapid development of printing technology, different types of printing technology and materials have appeared in recent years [57–62]. Printing is done mainly on the nanometer and millimeter scale. 3D material selection is also more extensive, covering a variety of polymers, metals, glass, and ceramics [63–66]. There are many kinds of printing materials, including powders, quantum dots, one-dimensional (1D) fibers or nanowires, two-dimensional (2D) nanosheets, and other structure-related materials [36,57,67–70]. Due to different structural characteristics, each kind of 3D-printing nanomaterial has unique properties and uses.

Based on the above description, extensive research and review has been performed on 3D-printing equipment, but most of it primarily concerns the development and application of electrolyte and printing technology. So far, there has been no comprehensive review of the materials, synthesis methods, and applications of related materials suitable for 3D printing. Therefore, we focused on a comprehensive review of various morphologies of nanomaterials, related electrochemical applications, and the latest progress and breakthroughs in the development of 3D-printing materials. First, the synthesis methods and morphologies of 3D-printing materials were discussed, including zero dimensional (0D), 1D, 2D, 3D structural materials, and other composite structure-related materials. The printing process, advantages and limitations of the synthesis methods, and morphology of each material were discussed (Fig. 1). Then, we discussed and compared the electrochemical applications and performance of printing materials such as electrodes and electrolytes for 3D printing. Finally, the current research status, future research trends, and challenges of 3D-printing materials are discussed.

2. 3D-printed materials

A 3D-printing ink with a high viscosity and shear thinning is important for successful 3D printing [71]. Although some electrochemically active materials have been used in 3D printing, their size and stability have caused many complications in 3D printing. Therefore, the development and utilization of new active materials and inks have become urgent. Herein, we briefly review the synthesis methods of several electrochemically active materials in 3D printing and some materials with potential applications in 3D printing.

2.1. Zero-dimensional 3D-printed materials

In the fields of telephony and energy storage, metals and metal oxides usually have a large theoretical capacity. Applying quantum dots to 3D printing can not only smoothen 3D printing, but also solve the problem of poor electrochemical performance of 3D-printing materials due to their slow ion and electron diffusion dynamics. Zhang *et al.* [72] prepared monodisperse SnO_2 quantum dots (QDs) on a large scale by a simple controlled sol-gel method (Fig. 2a). The material has a high specific capacity for electrochemical energy storage. Therefore, QDs are promising for 3D printing. Inspired by this, we summarize some typical QD synthesis methods. The synthesis of transition metal oxide QDs has been performed. For example, Soap free emulsion polymerization can not only effectively control the size, surface morphology and properties of colloidal particles, but also reduce the pollution and make clean materials, Tong *et al.* [73] synthesized Co_3O_4 QDs by the soap-free method and obtained Co_3O_4 QDs rich in oxygen defects by calcination under H_2/AR conditions. Liang *et al.* [74] synthesized KAS-ZnO QDs by combining kasugamycin (KAS) with aldehyde functionalized ZnO QDs *via* a shearable benzoimide covalent bond (Fig. 2b). In addition, some transition metal sulfide QDs have been synthesized. At the same time, in order to meet the specific needs of some material synthesis, different schemes can be adopted to synthesize different quantum dots. For instance, the required quantum dots can be synthesized *in situ* by using the original metal on a certain metal substrate. Yang *et al.* [75] prepared Co_9S_8 QDs based on the *in situ* selective sulfurization of Co on carbon fibers and embedded them into the interlayer of ternary metal layered double hydroxidenanosheets derived from metal organic frameworks. Quantum dots are synthesized *in situ* through the metal active sites in the raw materials, which further expands the synthesis method of quantum dots. In 3D printing technology, the successful extrusion of ink is closely related to the mechanical properties and morphology of the material. The existence of large size will not only destroy the shear stress required by the material in the extrusion process, but also block the needle in the extrusion process, which leads to the smooth printing progress being hindered. Therefore, the synthesis of small-size materials is very important. The size and morphology of materials can be further modified and controlled effectively by temperature control, cracking and etching, Wang *et al.* [76] successfully synthesized small-size ZnS QDs (2.5 nm) by a simple stirring hydrothermal pyroly-

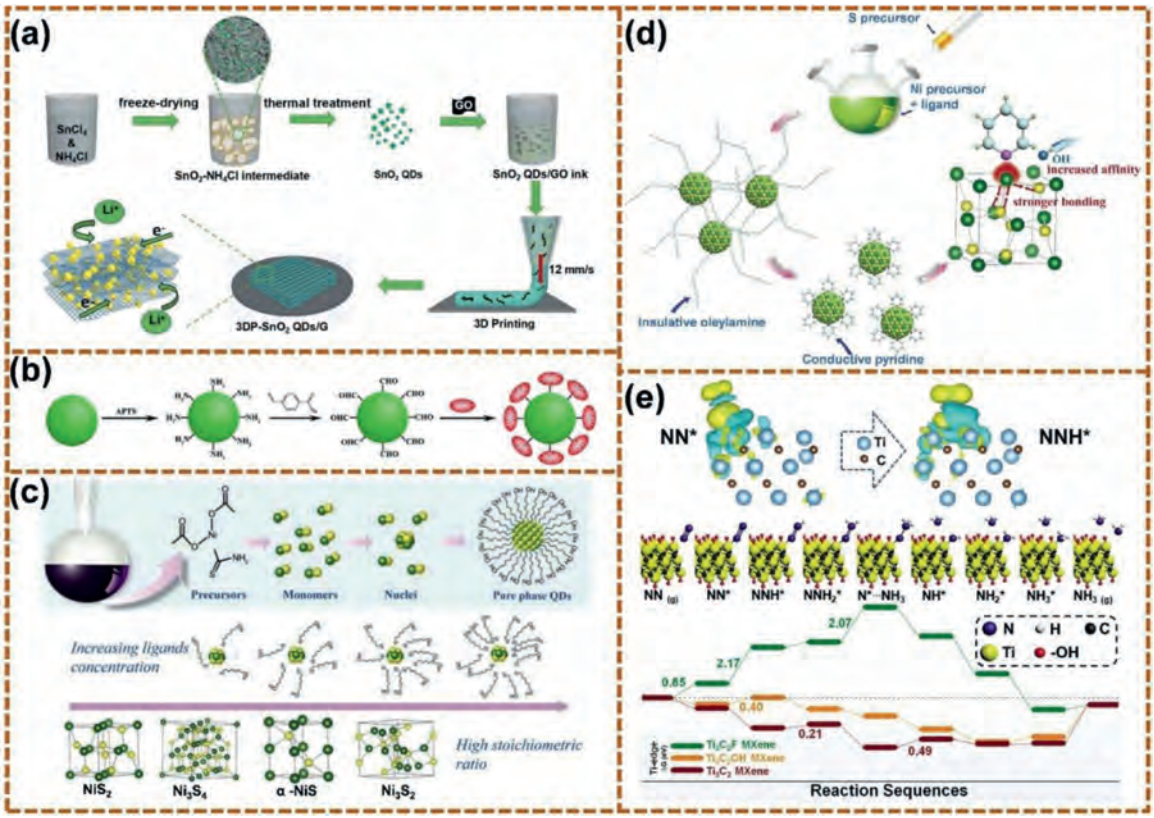

Fig. 2. (a) 3DP SnO_2 QDs/G architecture diagram. Copied with permission [72]. Copyright 2018, The Royal Society of Chemistry. (b) The formation mechanism of KAS ZnO quantum dots. Copied with permission [74]. Copyright 2019, Elsevier. (c) The formation mechanism of Ni_3S_4 quantum dots synthesized by one pot method and the effect of ligand concentration on the lattice structure of quantum dots. Copied with permission [78]. Copyright 2018, the Royal Society of Chemistry. (d) The synthesis strategy and mechanism of ligand induced effect on NiS_2 quantum dots. Copied with permission [79]. Copyright 2019, Elsevier. (e) Charge density difference, reaction mechanism diagram and free energy diagram. Copied with permission [82]. Copyright 2020, Wiley-VCH.

sis method. Sun *et al.* [77] synthesized edge-rich S-vacancy MoS_2 QDs based on the Lewis acid-base theory and top-down strategy. Chen *et al.* [78] synthesized monodisperse Ni_3S_4 QDs with an average size of 3.8 nm by the one-pot method (Fig. 2c). In the same year, Chen *et al.* [79] synthesized smaller NiS_2 QDs with an average size of less than 3.1 nm by a colloid injection method (Fig. 2d). In addition, Wu *et al.* [80] and Yuan *et al.* [81] have synthesized 3D pillared vanadium nitride (VN) QDs/CM composites and N-doped vanadium nitride QDs in porous shells of carbon hollow spheres by effective methods, respectively (VNQD@NC HSs). Jin *et al.* [82] successfully prepared Ti_3C_2OH QDs by alkalizing $Ti_3C_2T_x$ MXene in NaOH solution (Fig. 2e).

In summary, relatively small quantum dots (metals, metal oxides, metal sulfides, and metal nitrides) can be obtained by the sol-gel, soap-free, hydrothermal, and acid-base methods. However, although the synthesis of these methods further improves our requirements for the size and morphology of materials, some methods are complex and present some limitations in material synthesis. Therefore, in practical applications, further exploration of more mature and widely used quantum dot synthesis methods has vast application value.

2.2. One-dimensional 3D-printed materials

In the field of 3D-printing energy storage, metal oxide nanowires have been widely used, which can make it possible to print and control ink smoothly [83]. Through the regulation of hydrothermal temperature and hydrothermal time, the morphology of materials can be flexibly regulated. Therefore, hydrothermal synthesis of 1D nanowires has become a mature and effective method. Zhao *et al.* [84] synthesized V_2O_5 nanowires (NWs)/multiwalled carbon nanotubes (MWCNTs) with a 1D nanowire structure by hydrothermal synthesis, and VN NWs/MWCNTs by further annealing (Fig. 3a), additionally designing a 3D-printing coaxial fiber-shaped asymmetric supercapacitor (FASC) all-in-one device as positive and negative electrodes (Fig. 3b). The device has excellent mechanical properties and electrochemical stability. Yu *et al.* [85] developed a 3D-printing method for micro supercapacitors using carbon nanotubes. It can be further seen that 1D materials have a wide application prospect in the field of 3D printing technology. On this basis, we further reviewed several synthesis methods of V_2O_5 nanowires. André *et al.* [86] synthesized V_2O_5 nanowires *via* the hydrothermal method. Chen *et al.* [87] developed a hierarchical porous network structure composite comprising V_2O_5 nanowires and carbon nanotubes (Fig. 3c). In addition, Chen *et al.* [88] prepared nanocomposites with an interpenetrating network structure of fibrous carbon nanotubes and V_2O_5 nanowires *via* an *in situ* hydrothermal method. Other transition metal oxide nanowires have been synthesized. Yin *et al.* [89] synthesized MnO_2 nanowires *via* a hydrothermal method. Wan *et al.* [90] also synthesized MnO_2 nanowires by controlling the hydrothermal reaction time (Figs. 3f and g). Xiang *et al.* [91] prepared a 3D interlaced structure by uniformly combining MnO_2 nanowires deposited by atomic PD with CNTs (Fig. 3d). The micromorphology is shown in Fig. 3e.

1D nanowires have excellent flexibility and mechanical properties because of their interlaced structure, which has a good prospect for 3D printing. At the same time, a good network structure is conducive to ion exchange and transmission, giving it good electrochemical properties. The synthesis of a variety of metal oxide, nitride, and related composite nanowires by a simple hy-

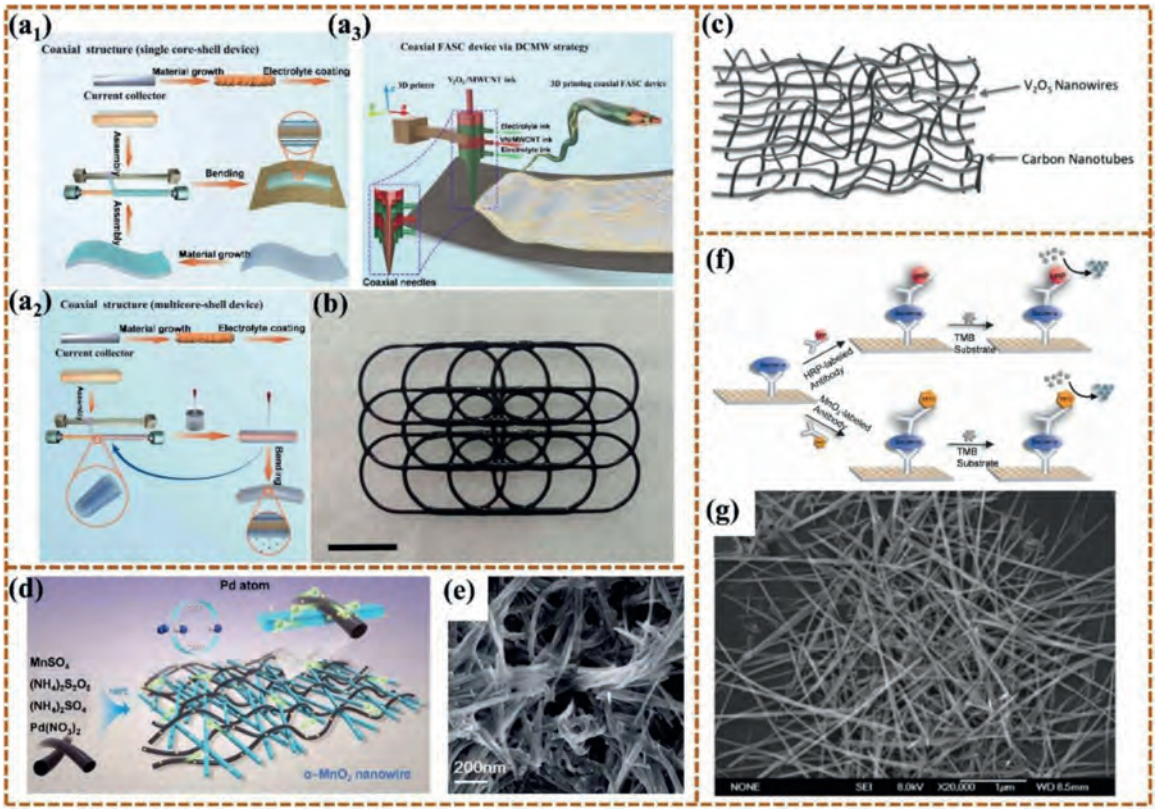

Fig. 3. (a) (a_1, a_2) The comparison of traditional FASC device and coaxial architecture fabrication process, and (a_3) the three-dimensional (3D) printing coaxial FASC device developed by our direct coherent multi ink writing (DCMW) technology. (b) DCMW 3D printing coaxial FASC device. (c) The method of forming supercapacitor materials based on the interpenetrating network of CNTs and V_2O_5 nanowires is illustrated. (d) Three dimensional staggered carbon nanotubes and platinum atom anchored a-MnO_2 nanowires for bifunctional OER and ORR electrocatalysis. (e) SEM image of Pd/MnO_2-CNT. (f) schematic diagram of bacterial detection method based on MnO_2 mediated immunoassay. The enzyme-labeled enzyme linked immunosorbent assay was proposed for comparison. (g) SEM images of MnO_2 nanowires. (a, b) Copied with permission [84]. Copyright 2018, Springer. (c) Copied with permission [87]. Copyright 2009, Wiley-VCH. (d, e) Copied with permission [91]. Copyright 2018, the Royal Society of Chemistry. (f, g) Copied with permission [90]. Copyright 2012, Elsevier.

drothermal and subsequent annealing method has been widely used.

2.3. Two-dimensional 3D-printed materials

2D materials, such as carbonaceous materials, conductive polymers, metal oxides, and metal sulfides, have high anisotropy, with transverse dimensions ranging from hundreds of nanometers to microns and a thickness of one nanometer. 2D materials have been widely used in various fields, particularly in the field of electrochemical energy storage, due to their high specific surface area, easy-to-control thickness and function, excellent electronic properties, mechanical strength, flexibility, and optical transparency. Controlling the assembly of these materials has a direct impact on their properties.

Graphene is one of the excitation materials for micro-sized electrical double-layer capacitors, water decomposition and solar cells due to its large surface area, high conductivity, good chemical stability, and other beneficial properties. However, due to the narrow channel, limited ion contact surface, and contact resistance, the stacking of graphene sheets notably affects its properties. At present, some attempts to create 3D carbon-based compressible devices have been made. The reduced graphene oxide method has been widely used because of its simple and effective operation, Nathan-Walleser *et al.* [92] obtained 2D sheet materials with excellent electrochemical properties by the thermal reduction of graphene oxide (TRGO) and introduced a simple 3D micro extrusion one-step printing process to manufacture five surfactant functionalized adhesive electrodes, which have a high charge–discharge performance. Zhu *et al.* [93] used GO and graphene nanoflakesas composite materials with high conductivity for printable composite ink without harmful surface area loss (Fig. 4a). In addition, in order to obtain the structure of special structural materials to further optimize the material structure, Jiang *et al.* [94] designed and manufactured 3D graphene aerogel microgrid by a simple ion-induced gel method (Fig. 4b), adding trace Ca^{2+} ions as an efficient crosslinking agent. This method adjusts the rheological behavior of ink by adjusting the interaction of GO sheets (Fig. 4c). Yao *et al.* [95] proposed a new surface-functionalized graphene aerogel (SF-3D GA) for 3D printing, which exhibits good dynamic properties and has a record high capacitance for independent carbon-based materials (Fig. 4d). In addition, the relationship between some related composites and other materials was also studied. At the same time, the composite materials formed by self-assembly between materials can effectively meet our needs in all aspects of materials. For example, Qi *et al.* [96] has prepared a superelastic polypyrrole (PPy)-coated GA electrode with a 3D framework with adjustable shape and periodic macropores by self-assembly (Fig. 4e). Zhao *et al.* [97] obtained mixed aerogel microgrid structure electrode materials by mixing ZnV_2O_6@$Co_3V_2O_8$ and VN with a 2D flake structure with graphene (Figs. 4f and g). These materials have good cycle stability and high specific capacitance when used in an asymmetric capacitor electrode.

In recent years, a class of 2D metal carbides and nitrides called MXenes has attracted increasing attention. The surface of MXene nanosheets carries negative charge, and the rich chemical composition of the surface makes it possible to form a stable and

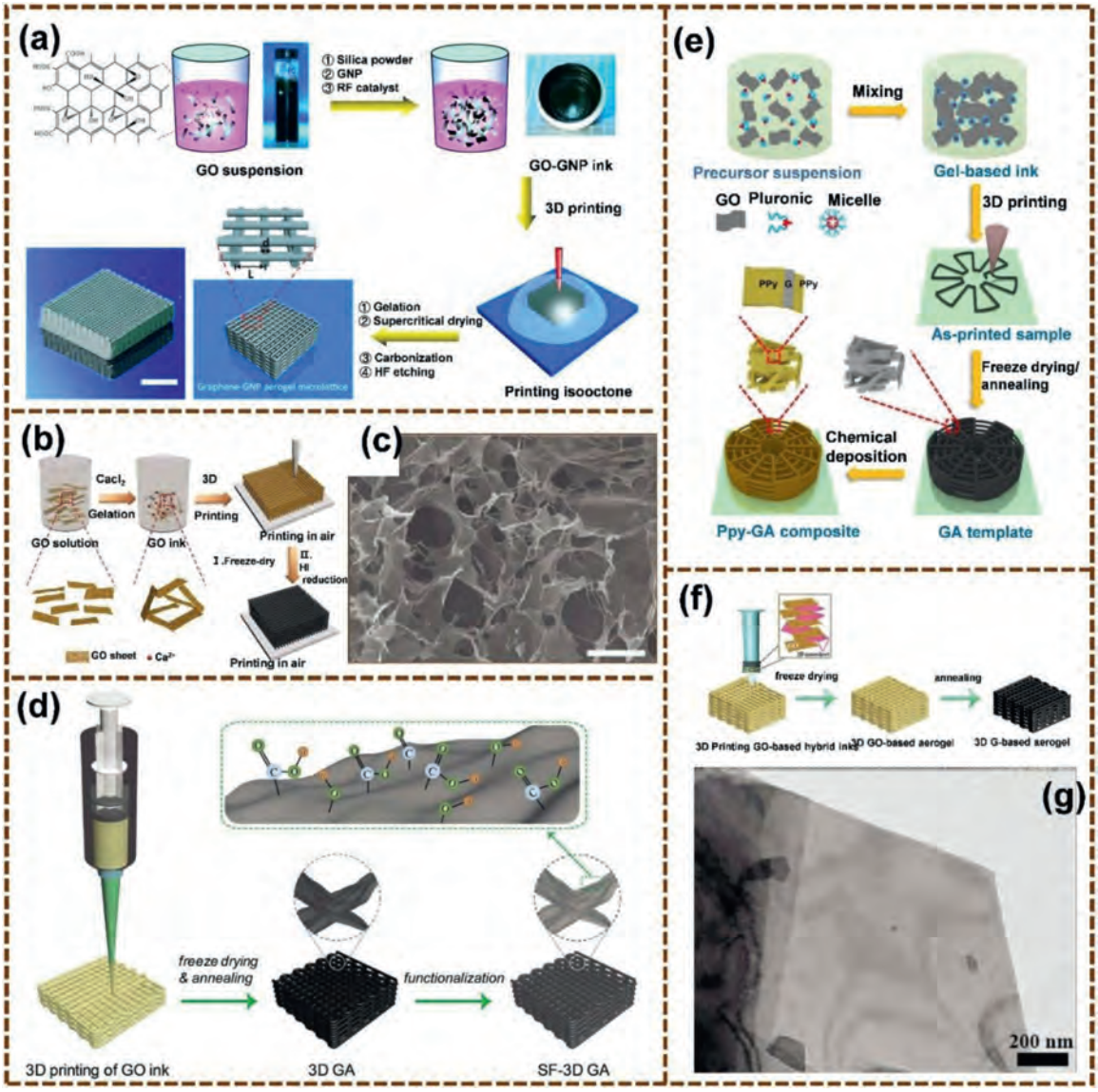

Fig. 4. (a) Manufacturing process diagram. (b) 3D printing process diagram (c) SEM images and structural analysis of graphene oxide and graphene microcrystal lattice were printed neatly. (d) SF-3D GA production diagram. (e) Three dimensional layered PPy GA composite preparation process diagram. (f) Schematic illustration of as-fabricated 3D printing 3D G-based aerogel electrode. (g) ZnV_2O_6@$Co_3V_2O_8$ TEM images of lamellar structure. (a) Copied with permission [93]. Copyright 2016, American Chemical Society. (b, c) Copied with permission [94]. Copyright 2018, Wiley-VCH. (d) Copied with permission [95]. Copyright 2019, Wiley-VCH. (e) Copied with permission [96]. Copyright 2018, Wiley-VCH. (f, g) Copied with permission [97]. Copyright 2019, Wiley-VCH.

adhesive colloidal water solution without any surfactant or polymer. Yang *et al.* [98] developed additive-free 3D-printing ink based on thin $Ti_3C_2T_x$ nanosheets with a large transverse size to form a strong solid $Ti_3C_2T_x$ network with ideal rheological properties, which can be used to print independent 3D structures layer by layer (Fig. 5a). Orangi *et al.* [99] introduced the use of viscoelastic, high concentration, water-based, and additive free MXene ink, which is the best choice for the preparation of a 3D-printing all-solid-state micro supercapacitor (3D MSCs) electrode material. Fan *et al.* [100] uses micro M^{2+} (such as Zn^{2+}) as an auxiliary gel strategy instead of high-dose external additives, which further enhances the interaction between MXene nanosheets and effectively suppresses the stacking of MXene nanosheets. Therefore, Ti_3C_2 MXene gel ink with good rheological properties is directly used for 3D printing (Fig. 5d). Yu *et al.* [101] doped nitrogen into MXene by a melamine formaldehyde template method to enhance its redox activity and conductivity to improve its electrochemical performance (Fig. 5b). The design of the two kinds of MXene-N-based inks with different viscosities was demonstrated to build a printable electrochemical energy storage device. Zhang *et al.* [33] demonstrated a simple, low-cost, and novel stamping strategy, and quickly created high-performance, coplanar solid-state $Ti_3C_2T_x$ MXene MSCs by combining 3D printing with viscous MXene water-based ink. Cain *et al.* [102] realized the formation, assembly, and blocking of MXene nano sheet surfactant at the oil–water interface through the interaction of an amine terminal ligand and the inherent surface functionalization and negative charge on a $Ti_3C_2T_x$ sheet, and prepared the 3D modeling of planar MXene film and a two-phase liquid mixture. In addition, transition metal oxide nanosheets are also widely used in 3D printing. For example, Shen *et al.* [103] first developed a 3D-printing method to prepare quasi-solid asymmetric mesenchymal stem cells using vanadium pentoxide (V_2O_5) nanosheets and graphene vanadium nitride quantum dots (G VNQDs) as cathode and anode inks, respectively (Fig. 5c). Cai *et al.* [104] proposed a two-in-one strategy to prepare dual-functional V_8C_7-VO_2 heterostructure scaffolds based on

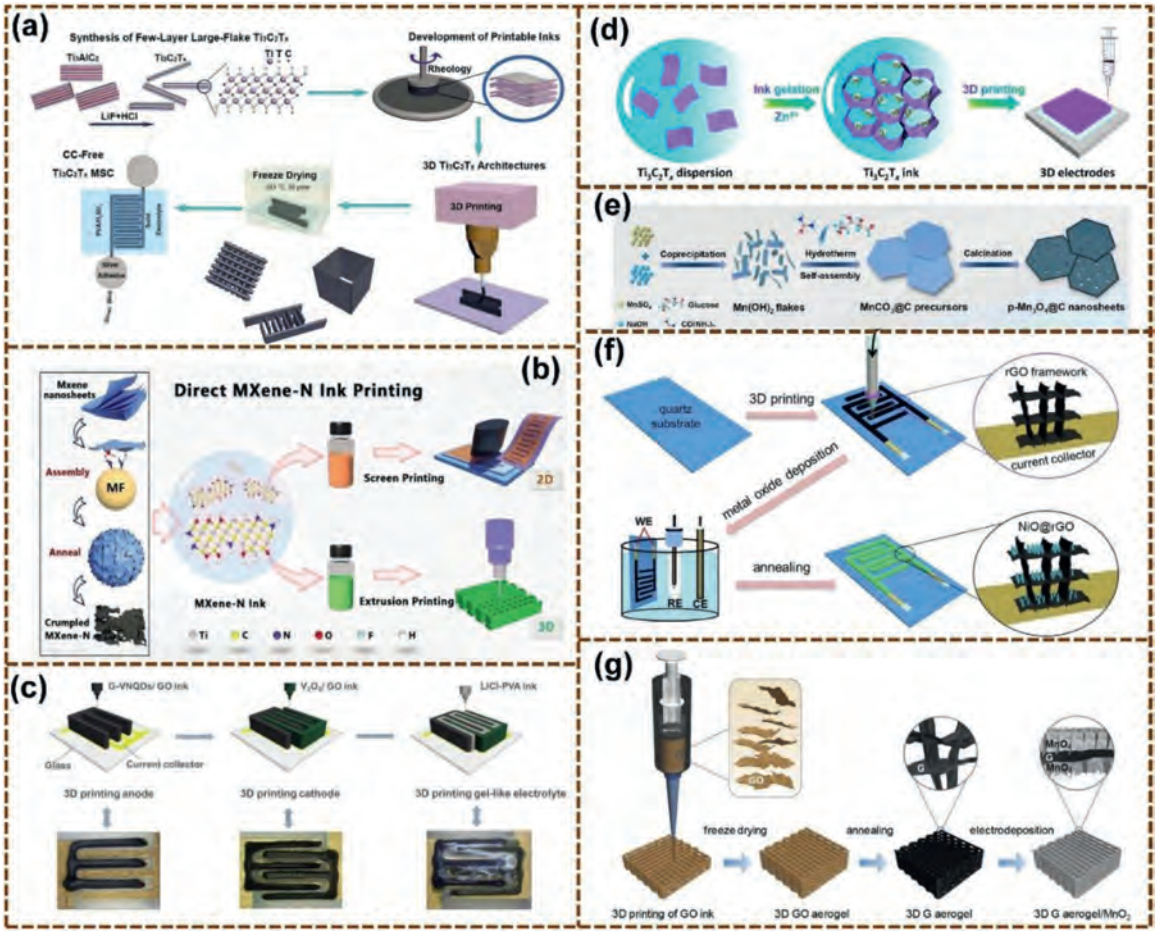

Fig. 5. (a) Independent MXene architecture and MSc demonstration of 3D printing manufacturing strategy diagram. Copied with permission [98]. Copyright 2019, Wiley-VCH. (b) Direct MXene-N ink printing schematic. Copied with permission [101]. Copyright 2019, Wiley-VCH. (c) 3D printing schematic diagram of asymmetric MSC with interdigital electrodes. Copied with permission [103]. Copyright 2018, Wiley-VCH. (d) The preparation principle diagram of bivalent ionization mxene ink and 3DP MXene electrode. Copied with permission [100]. Copyright 2021, American Chemical Society. (e) Pure Mn_3O_4 and p-Mn_3O_4@C Typical synthesis of nanosheets. Copied with permission [105]. Copyright 2021, the Royal Society of Chemistry. (f) 3D printing can be used to manufacture the schematic diagram of NOG based quasi solid state MPC interconnection framework. Copied with permission [106]. Copyright 2019, Elsevier. (g) 3D printed graphene aerogel/MnO_2 electrode production schematic diagram. Copied with permission [108]. Copyright 2019, Elsevier.

3D printing. Peng *et al.* [105] synthesized porous carbon-coated hexagonal Mn_3O_4 (p-Mn_3O_4@C) nanoplates *in situ* that were used as electrodes (Fig. 5e). Structure can effectively improve conductivity and electrochemical stability. Wang *et al.* [106] developed an interdigitated graphene framework (IGF) structure with a unique open porous interconnection support and a required microelectrode mode through simple extrusion 3D printing. MPCs were prepared by filling MnO_2 nanosheets supported by an IGF structure (Fig. 5f). Wang *et al.* [107] synthesized a new flexible and unbonded paper composite of Mn_3O_4/reduced GO nanosheets by ultrasonic crushing, filtration, and hydrothermal reduction. The large specific surface area and abundant pores of the composite provide more electrochemical active centers for electrons and ions. In addition, interconnected nanostructures can also effectively inhibit the self-condensation of rGO NSS. Yao *et al.* [108] deposited manganese oxide (MnO_2) on the collector by electrodeposition. A 3D-printed graphene aerogel/MnO_2 electrode has a highly porous structure and is conducive to the effective diffusion of ions (Fig. 5g). Liu *et al.* [109] designed a complete and ordered porous 3D copper conductive framework using 3D direct ink-writing technology and prepared a CuO nanosheet array by an *in situ* electro oxidation method. This porous structure can effectively improve the surface area and enhance the permeability of the electrolyte, thus further promoting the effective transport of ions and electrons.

In conclusion, 2D materials have been widely used in the field of 3D printing. It can be concluded that the most commonly used 2D materials are graphene-based, transition metal carbonitrides, and a small amount of transition metal oxide nanosheets. Due to the limitation of materials and 3D-printing requirements, the application of 2D materials in 3D printing needs further development and research.

2.4. Three-dimensional 3D-printed materials

Most materials with three-dimensional structure are synthesized in powder state, and the 3D structure materials have large size. When applied to 3D printing, it will cause particle scattering, material loss and needle blockage. However, 3D materials usually have large specific surface area and more electrochemical active sites. Therefore, it is of great significance to incorporate 3D structural materials in 3D printing technology. Nowadays, metal organic frameworks (MOFs) applied for 3D printable materials are usually formed by suspending pre synthesized ions in ink and further processing [110]. However, MOFs do not combine well with binders, which results in poor rheological properties of the ink. To solve this problem, Lawson *et al.* [111] used a gel-printing growth monomer to print an MOF gel precursor through 3D to coordinate MOF, synthesized a sol-gel containing 70% HKUST-1 precursor, and

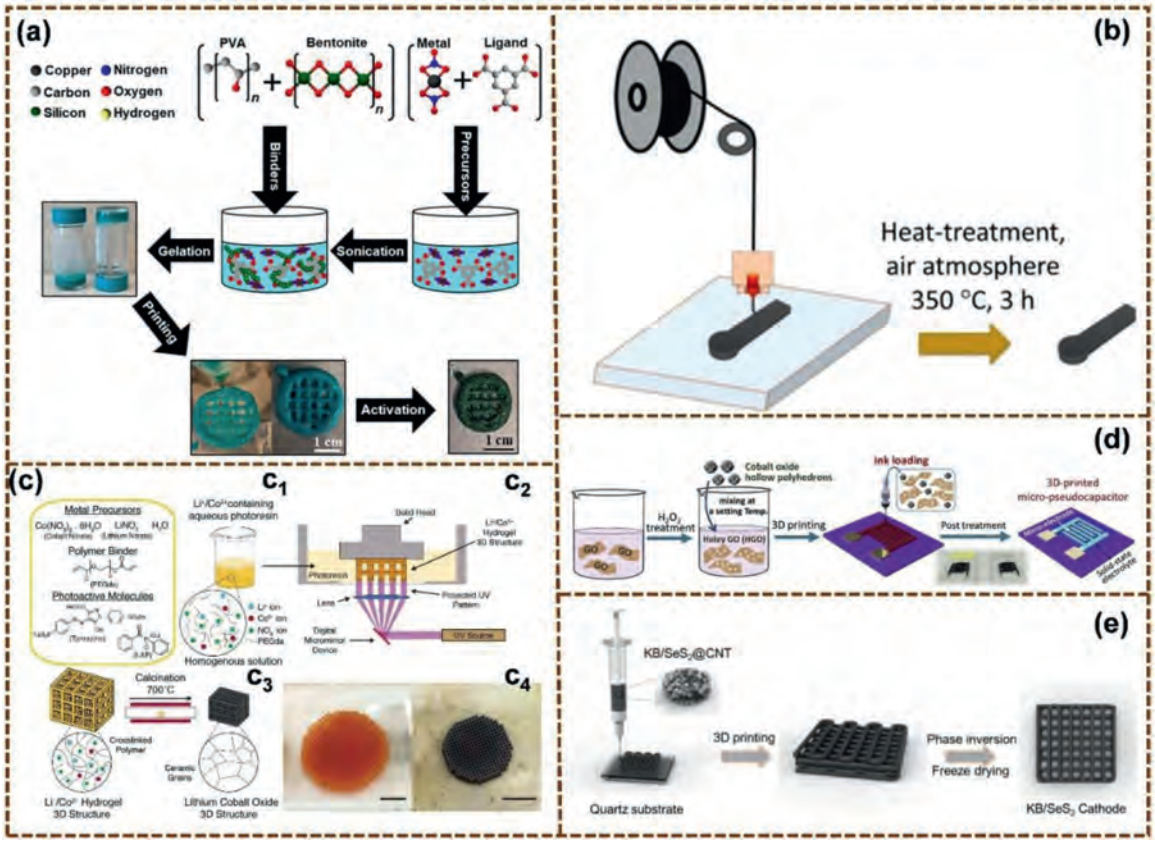

Fig. 6. (a) Schematic diagram of HKUST-1 monolithic stone prepared by new gel-print-grow (GPG) technology. Copied with permission [111]. Copyright 2020, American Chemical Society. (b) 3D printing (melt deposition modeling) technology and printing electrode activation diagram. Copied with permission [114]. Copyright 2020, Wiley-VCH. (c) DLP printing water-based metal salt containing light resin. (c_1) Resin formulation and schematic diagram of polyethylene glycol solvated metal ions in aqueous light resin. (c_2) DLP printing sketch of Li^+/Co^{2+} hydrogel three-dimensional structure. (c_3) Calcined 3D Li^+/Co^{2+} hydrogel to form a self-similar LCO structure. (c_4) Optical images of Li^+/Co^{2+} hydrogel (left) and calcined LCO (right) cubic lattice. Scale, 5 mm. Copied with permission [116]. Copyright 2020, Wiley-VCH. (d) 3D printing process diagram of quasi solid planar rHGC MPCs. Copied with permission [117]. Copyright 2019, Elsevier. (e) Extrusion 3D printing of cell structure of selenium disulfide/ketjenblack composite. Copied with permission [120]. Copyright 2020, Elsevier.

optimized the *in situ* growth conditions by changing the activation solvent and the dissolution temperature (Fig. 6a). Zhong *et al.* [112] used extrusion 3D printing to implant nano-ZIF-8 into composite polycaprolactoneand calcium dihydrogen phosphatescaffolds to prepare composite scaffolds with a uniform structure, high mechanical strength, and high macroporous connectivity. Ying *et al.* [113] transformed octahedral ZIF-67 into active porous metal oxide Co_3O_4 nanosheets by a controlled electrochemical method. The material was directly coated onto the surface of a 3D-printed titanium (Ti) electrode to form a ZIF-67/Ti-E electrode by a mild step-by-step *in situ* growth method. Graphene/polylactic acid (PLA) filaments are widely used in melt manufacturing. Recently, Ghosh *et al.* [114] doped titanium oxide and iron oxide into graphene/PLA filaments to fabricate 3D-printed electrodes (Fig. 6b). This discovery allowed other active materials to be introduced into the filament in a controllable way, which can be used to customize high-performance 3D-printed electrodes. Santos *et al.* [115] electrodeposited PLA/graphene electrode with low-cost nickel iron hydroxide containing oxygen, effectively improving the activity of the electrocatalytic oxygen evolution reaction (OER) in an alkaline medium. To optimize electrochemical performance, the composition of the electrocatalytic surface can be adjusted by the relative content of nickel and iron in the electrodeposited solution. Yee *et al.* [116] avoided the addition of 3D multi-component metal oxides using an aqueous metal salt photocatalyst, and the manufacturing method depended on the particle type or the organic-inorganic binder, which was limited in chemical composition and resolution, respectively (Fig. 6c). Through the synthesis of a homogeneous lithium and cobalt nitrate solution resin and printing with digital light treatment, a hydrogel containing lithium and cobalt ions was obtained, and a lithium cobalt oxide (LCO) structure was constructed. Tian *et al.* [117] combined an exfoliated porous graphene oxide (HGO) sheet with pseudocapacitive cobalt oxide hollow nano polyhedrons and prepared a high concentration composite ink without additives (Fig. 6d). The ink used in 3D printing has good rheological properties, such as shear dilution, and a non-Newtonian and steady flow. An MPC microelectrode supported by reduced HGO was constructed by 3D printing and freeze-drying. Figueredo-Rodriguez *et al.* [118] mixed Fe_2O_3 nanopowder, carbon powder and Bi_2S_3 powder balls to form an iron electrode by 3D printing, which has a high energy density when applied to a water-iron-air battery. Saleha *et al.* [119] printed nanoparticle dispersed droplets directly, then heated them to remove solvents and sinter the nanoparticles, resulting in a large porosity, thus forming a hierarchical porous system with a very high surface-to-volume ratio. A highly complex high-capacity high-strength microcrystalline lattice electrode Li ion battery was fabricated by 3D printing. Shen *et al.* [120] used low-cost commercial ketjenblack (KB) with rich meso– and microporosity as the matrix material of SeS_2, and used extrusion-based 3D printing to fabricate hierarchical freestanding honeycomb microgrid electrodes for Li ion batteries (Fig. 6e).

2.5. Others

Various material morphologies are used in 3D printing. Due to its rich amphiphilic, stable dispersion and tunable rheological properties, 2D materials are often selected to prepare various aqueous composite inks. For different printing purposes, the rheological properties required by printing inks are controlled by changing the concentration and proportion of 2D material inks and additives (such as Ca^{2+}, CNTs and cellulose nanofibers), such as good formability high porosity, excellent conductivity, and mechanical stability. So far, a variety of electrode structures based on different morphologies have been successfully designed and constructed, such as mesh, cross and micro dot array structures [121–123]. Kong *et al*. [124] synthesized CNTs (1D) and rGO nanosheets (2D) through simple solvothermal and direct ink writing techniques for the printing of self-supporting and thickness-adjustable periodic rGO/CNT hybrid aerogel microcrystals. Through reasonable design and adjustment of chemical composition, we directly grow α-Fe_2O_3 nanorods and Ni-$(OH)_2$ nanosheet arrays on an rGO/CNT surface (Fig. 7a). As an ink for 3D printing, this material has ideal shape, size, and high dispersion. Tang *et al*. [125] prepared high-concentration printable electrode inks by mixing Fe_2O_3 nanoparticles, 1D silver NWs, and 2D graphene nanoparticleswith adhesives. The resulting electrode ink shows good printing performance and can be processed by extrusion (Fig. 7b). The 3D-printed MSCs have high device area capacitance, high energy density, and good cycle stability. Zhou *et al*. [126] used a simple ion-induced gel method to transform a GO sol into hydrogel by adding $CoCl_2$ as a crosslinking agent in a chemical crosslinking reaction between cobalt ions and oxygen functional groups on GO sheets. A graphene film electrode with controllable shape and structure was prepared to match the rheological properties of 3D printing. This method avoids the shortcomings of the pure oxygen graphene ink, such as insufficient viscosity and complicated production procedure. Nitrogen-doped graphene was prepared by annealing in 1 mol/L urea solution to improve the conductivity of graphene. Gao *et al*. [127] used 2D reduced GO nanosheets as adhesive and support, 3D AC microparticles as active materials, and 1D CNTs to form a conductive network (Fig. 7c). A compact 3D brick-like activated carbon/1D carbon nanotube/reduced graphene oxide (AC/CNT/rGO) carbon composite electrode with adjustable thickness is formed without using a polymer adhesive, and the layered extrusion 3D printing is used for high-energy density supercapacitors. Shen *et al*. [128] designed a 3D sulfur copolymer graphene system with a periodic microcrystalline lattice, high viscosity, and shear thinning characteristics using the formulation of sulfur particles, 1,3-diisopropyl benzene (DIB), and concentrated GO dispersion and extrusion 3D printing (Fig. 7d). The sulfur copolymer can be formed by heat treatment through the reaction of elemental sulfur and DIB. Some of them can inhibit the dissolution of polysulfides. In addition, the presence of graphene can also provide a high conductivity for the whole electrode. Li *et al*. [121] introduced a simple strategy to utilize 3D printing and unidirectional frozen pseudoplastic nanocomposite gels (Fig. 7e) by preparing a viscous pseudoplastic nanocomposite ink composed of $Ti_3C_2T_x$ nanosheets, manganese dioxide nanowires (MnONWs), silver nanowires (AgNWs), and fullerenes (C60) (Fig. 7f). A high-resolution thick honeycomb porous cross-electrode and essentially stretched mesenchymal stem cells were constructed. Zhang *et al*. [123] introduced a new strategy for manufacturing all-printed solid-state micro supercapacitors with a multilayer structure through multi-material 3D printing. Polypyrrole/polyaniline (PPy/PANI) coaxial nanotubes were synthesized by self-degradation template polymerization and *in situ* electrochemical polymerization. The ink based on polymer/graphene is environmentally friendly, safe to dry, low-cost, and versatile. Tang *et al*. [129] enhanced the viscoelastic response of the solution by introducing sodium alginate into GO solution and adopted the newly developed $Ni_{0.33}Co_{0.66}(OH)_2{\cdot}xH_2O$, which is ultra-fine and has high stability. Through this 3D-printing strategy, $Ni_{0.33}Co_{0.66}S_2$/type graphene aerogels with highly interconnected and programmable internal network modes were constructed. Azhari *et al*. [130] introduced the application of bonded spray powder bed technology in the fabrication of thick graphene-based 3D structures, which directly uses the high specific surface area powder produced in the rapid thermal expansion process of GO. The heat generated by the surface polymerization between wrinkles and folds reduces the contact resistance between the powder agglomerates by modifying the TRGO sheet with Pd nanoparticles. Rocha *et al*. [131] used additive manufacturing technology to manufacture electrodes. The device uses copper as the collector and chemically modified graphene (CMG) as the active material for the preparation of Pluronic F127 hot ink. These formulations are water-based, nontoxic, flexible, easy-to-upgrade, and easy-to-design inks, containing materials with different shape, size, chemical composition, and surface area, from 2D materials (CMG) to metal particles (Cu), with optimized rheological behavior, and multi-material devices for 3D printing. Yu *et al*. [132] produced heavy-duty NiCoP/MXene (NCPM) electrodes by the *in situ* growth of NiCoP bimetallic phosphide nanowires on the surface of Ti_3C_2 MXene nanosheets and designed an ASC device with a printed NCPM positive electrode and a printed AC negative electrode. The NCPM electrode has layered holes and an adjustable mass load, resulting in thorough electrolyte penetration and convenient charge transfer, improving cycle stability and rate capability.

3. Electrochemical application

With increasing demand for portable electronic devices, the development of small energy storage systems is urgent. 3D direct printing ink writing technology has been successfully used to construct complex structures. 3D printing is widely used in various fields, such as electronic equipment, biotechnology, engineering composite materials, and energy storage devices due to its continuous good manufacturing capacity, low cost, and flexibility. Electrochemical performance depends on electrode manufacture and structure, the type of the electrolyte, and the active material.

3.1. Supercapacitors

Supercapacitors, which have the advantages of high power density and charge storage capacity, excellent low temperature performance, long life, and fast charge and discharge, have become one of the most promising energy storage devices in the application of 3D-printing technology. Zhao *et al*. [84] designed a 3D-printing coaxial FASC all-in-one device with V_2O_5 NWs/MWCNTs and VN NWs/MWCNTs as positive and negative electrodes, respectively. The device has excellent mechanical properties and flexibility. After 5000 cycles of repeated bending, the capacitance retention rate can reach 95.5%, which is superior to asymmetric supercapacitors with a traditional coaxial structure (87.1%) and twisted structure (78.2%) (Fig. 8a). Ma *et al*. [133] proposed a novel reversible self-protecting micro-supercapacitor based on a thermally responsive polymer electrolyte to prevent thermal runaway. Yu *et al*. [85] used 3D printing, pre-designed base temperature, and a pre-programmed printing track to make the electrode, which can improve the structural integrity of the motor. The 3D-printed MSC device has good cycle stability and reliable energy storage capacity, which indicates that the micro power supply device is promising for energy storage applications. Zhang *et al*. [123] reported a new strategy for the scalable fabrication of all-printed solid-state micro supercapacitors with multilayer structures by multimaterial 3D printing. One option is to print the electrode directly onto tape

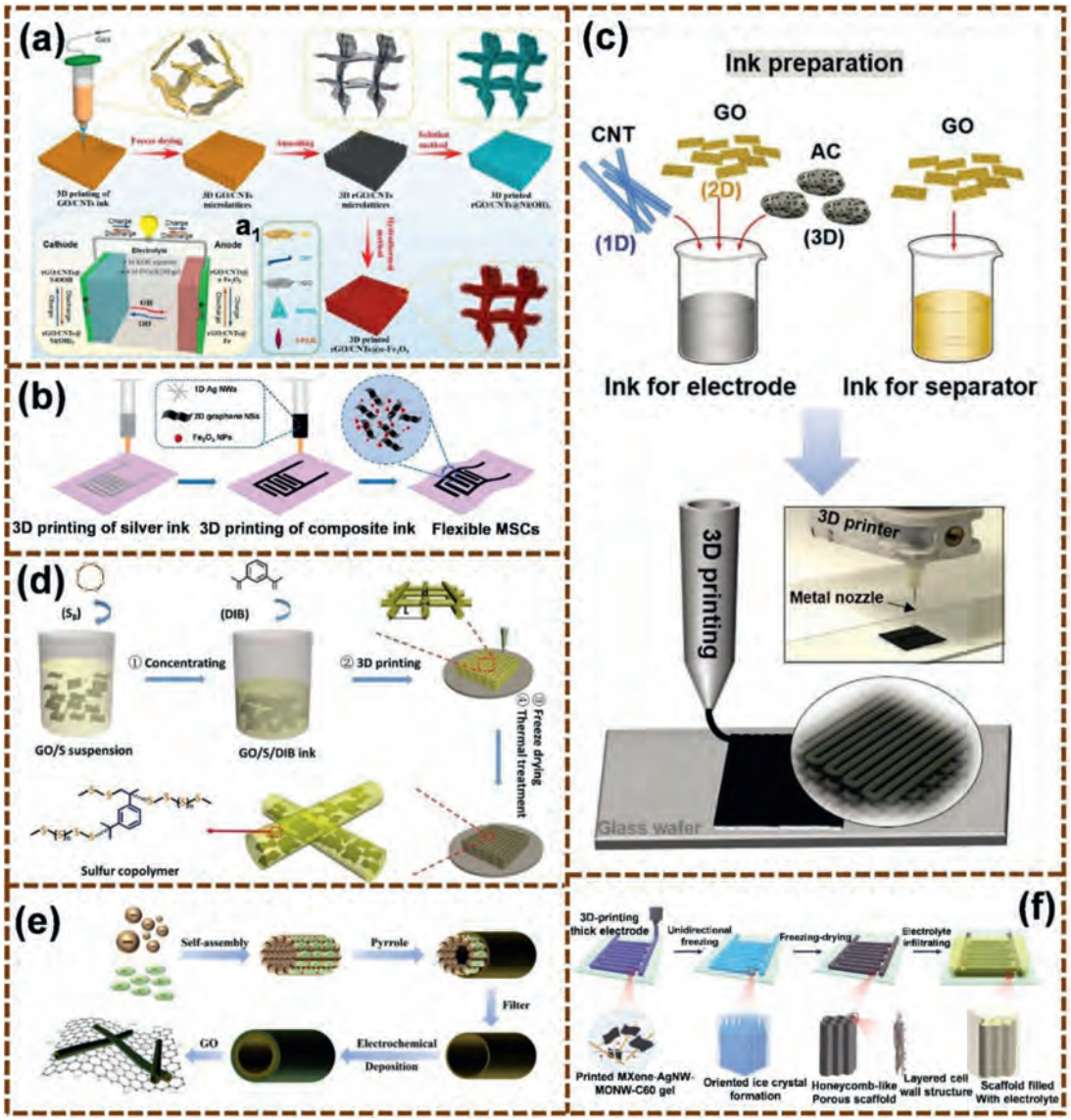

Fig. 7. (a) 3D printing process and schematic diagram of Ni−Fe Battery. Copied with permission [124]. Copyright 2020, American Chemical Society. (b) The DIW process diagram of Fe_2O_3/graphene/Ag electrode 3D printing flexible MSCs. Copied with permission [125]. Copyright 2020, Virtual and Physical Prototyping. (c) 3D printing of carbon composite electrode and separator. Copied with permission [127]. Copyright 2018, Wiley-VCH. (d) 3D printing sulfur copolymer graphene (3D-PSG) system structure demonstration. Copied with permission [128]. Copyright 2017, Wiley-VCH. (e) Schematic diagram of electrode ink formation. Copied with permission [123]. Copyright 2018, Elsevier. (f) The process diagram of MSC with essential extensibility was prepared by 3D printing and unidirectional freezing. Copied with permission [121]. Copyright 2020, Wiely-VCH.

to make a transferable device. The other is a wearable MSC prepared *in situ*, which has good performance and excellent flexibility and can be printed directly onto a lab coat. As shown in Figs. 8b and c, the multilayer MSCs show excellent electrochemical performance: the four-layer device has a high surface capacitance (151.2 mF/cm^2), with maximum bulk energy density at 19.6 mWh/cm^3 when the average power density is 0.91 mW/cm^3. Li *et al.* [121] used thick honeycomb porous cross-electrode 3D printing to construct stretchable mesenchymal stem cells. The electrochemical reaction mechanism of the device is shown in Fig. 8d. An MSC has good rate performance and long-term cycle stability. At 50% tensile strain, the area capacitance degradation of an MSC is less than 20%; however, it still maintains 75% of the initial capacitance after 1000 tension/release cycles. Tang *et al.* [129] first demonstrated a dual-electrode hybrid EES device constructed using 3D printing. The device has a high surface capacitance, excellent rate performance, and good cycle stability. Fig. 8g shows the excitation diagram of the electrochemical reaction of the device sample. As shown in Fig. 8f, after charging and discharging 10,000 times, 87.6% capacitance is retained. This 3D-printing method can be easily extended to other materials (functional nanomaterials/graphene composite aerogels) and provides a powerful platform for energy conversion and storage, MEMS, biomedical electronics, and environmental remediation. Tian *et al.* [117] proposed a 3D-printing strategy based on extrusion. As shown in Fig. 8e, a 3D-printed microelectrode with a high conductivity and a continuous ion transport channel was obtained by the surface modification of GO nanosheets. The electrode has a high capacitance, excellent rate performance, and strong cycle stability (91% capacity retention after 11,000 cycles). In addition, Shao *et al.* [134] prepared a high 1T ultra-thin c-MoS_2 material by an electrospray method and made it into a binder-free functional ink through ink adjustment to expand an inkjet printing MSC device. The 3D 1T cMoS_2//rGO asymmetric micro-supercapacitors (AMSCs) assembly

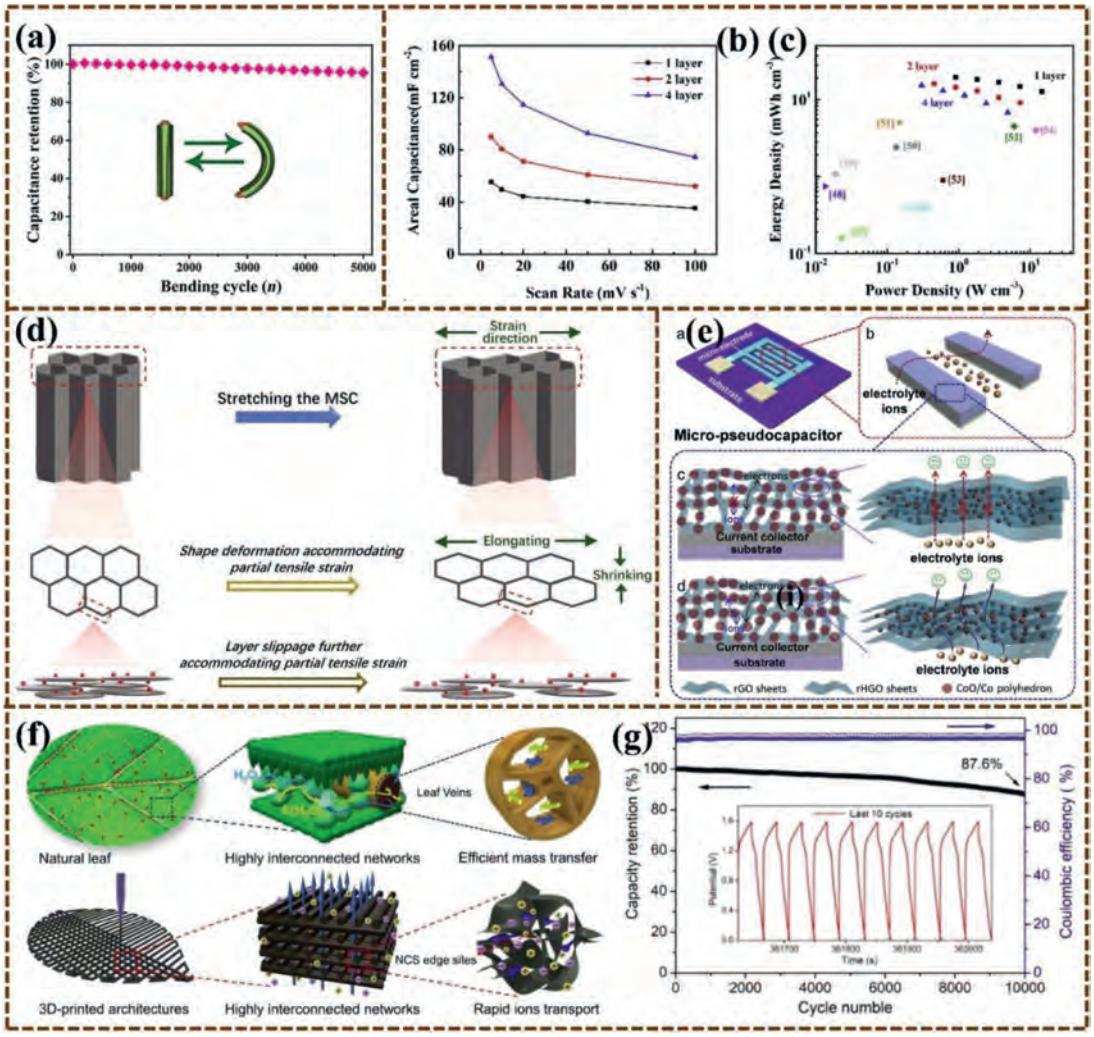

Fig. 8. (a) V_2O_5 NWs/ MWCNTs and VN NWS/MWCNTs were used as positive and negative devices respectively for capacitance retention after 5000 cycles. (b) The area capacitance of the device with different layers is a function of the scanning rate. (c) Ragone plot of full print multi-layer MSCs and recent literature reports. (d) 3D printing of deformation of honeycomb scaffold and layer slip of layered cell wall of thick interdigital electrode under tensile strain in MSC equipment. (e) Schematic diagram of capacitive charge storage mechanism of RGC and rHGC MPCs. (f) schematic diagram of mass transfer process of natural leaves and 3DP-NCS/G aerogel electrodes. (g) Cycling stability was measured at 100 mA/cm^2. Inset: the last ten cycles of the GCD curve. (a) Copied with permission [84]. Copyright 2018, Springer. (b, c) Copied with permission [123]. Copyright 2018, Elsevier. (d) Copied with permission [121]. Copyright 2020, Wiley-VCH. (e) Copied with permission [117]. Copyright 2019, Elsevier. (f, g) Copied with permission [129]. Copyright 2018, Wiley-VCH.

device have a stable working voltage of 1.75 V and an excellent cycle stability in a $MgSO_4$ aqueous solution. Chao *et al.* [135] synthesized soluble MoS_2/PEDOT:PSS (MP) hydrogels directly from PEDOT:PSS, Na_2MoO_4, and L-cysteine precursors using a simple synthetic method (one-pot hydrothermal method). MP has a stable dispersion in water, can be used for vacuum filtration and 3D extrusion printing, and has a wide application potential. For supercapacitors, maintaining a fast-charging capacity at low temperatures is a major challenge. Yao *et al.* [136] studied the important role of multi-scale open 3D porous structures in realizing the performance of ultra-low temperature supercapacitors. It is proven that the 3D-printing carbon aerogel with an open porous structure has a higher energy storage capacitance than non-3D block aerogels at ultra-low temperatures. Kang *et al.* [137] easily achieved excellent load density and area capacitance by establishing a double continuous transmission path of ion/electron species and a self-healing mechanism to eliminate interface resistance. Xiao *et al.* [138] directly produced ionic liquid electrolyte films with a digital inter-pattern by depositing phosphorus nanosheets layer-by-layer and electrochemically stripping graphene, and directly transferred them to a polyethylene terephthalate substrate. The device has an excellent electrochemical performance. Liu *et al.* [139] successfully wound functional nanowires and crosslinking agents (2D nanosheets, GO and MXene nanosheets) into nanowire junctions as crosslinking materials. Finally, a functional nanowire gel was 3D-printed, and an MSC subdevice was successfully prepared. Zhao *et al.* [140] used advanced 3D printing to integrate temperature sensors with FASC. In the FASC device, the positive pole of V_2O_5/SWCNT fibers and the negative pole of VN/SWCNT fibers are distorted. The FASC device has a high specific capacitance and an excellent mechanical flexibility (116.19 mF/cm^2 at 0.6 mA/cm^2). Fan *et al.* [141] assembled a 3D-printed hybrid capacitor and sodium ion hybrid capacitor device with a high energy and power density using porous nitrogen doped MXeneas the anode material and activated carbon as the cathode material. The ink used in the device has the advantage in that it can print directly to form an electrode structure without the use of a collector.

To summarize, the application of 3D printing in the field of micro supercapacitors is mature (Table 1). 3D-printed lattice structures can significantly reduce ion diffusion resistance and distance,

Table 1
Application of 3D printing materials in supercapacitors.

Sample	Electrolyte	CD/SS	SC	ED	PD	Ref.
TRGO	1 mol/L KOH	15 V/s	4 F/cm^3	4.43 mWh/cm^3	42.74 kW/cm^3	[92]
CNTs	–	20 μA/cm^2	2.44 mF/cm^2	0.12 mWh/cm^3	3.72 W/cm^3	[85]
V_2O_5 NWs/MWCNTs	KOH	1 mA/cm^2	152.7 mF/cm^2	54.3 Wh/cm^2	801.4 W/cm^2	[84]
PPCANT-rGO	0.01 mol/L H_2SO_4	0.48 mA/cm^2	151.2 mF/cm^2	19.6 mWh/cm^3	0.91 mW/cm^3	[123]
Mn_3O_4 NSs/rGO	6 mol/L KOH	0.5 A/g	409 F/g	–	–	[107]
3D-GCAs	3 mol/L KOH	10 A/g	63.6 F/g	0.26 Wh/kg	4079.9 W/kg	[93]
G/MnO_2	3 mol/L LiCl	1 mA/cm^2	18.74 F/cm^2	1.56 mWh/cm^2	–	[108]
ZnV_2O_6@$Co_3V_2O_8$	1 mol/L KOH	0.5 A/g	149.71 F/g	52.64 Wh/kg	394.88 W/kg	[97]
GO	1 mol/L H_2SO_4	0.5 A/g	213F/g	–	–	[94]
VO_x/rGO	5 mol/L LiCl–PVA	0.63 mA/cm^2	207.9 mF/cm^2	43.1 μWh/cm^2	3.77 mW/cm^2	[103]
2D $Ti_3C_2T_x$	sulfuric acid	1.7 mA/cm^2	2.1 F/cm^2	0.0244 mWh/cm^2	0.64 mW/cm^2	[98]
$Ti_3C_2T_x$ MXene	PVA/H_2SO_4	2 mV/s	1035 mF/cm^2	56 mWh/cm^3	24.9 W/cm^3	[99]
3DP Cu@CuO	KOH	30 mA/cm^2	1.690 F/cm^2	–	–	[109]
3DP MXene	0.03 mol/L $ZnSO_4$	10 A/g	184.4 F/g	0.10 mWh/cm^2	5.90 mW/cm^2	[100]
AC/CNT/rGO		10 mV/s	9.16 F/cm^2	0.63 mWh/cm^2	–	[127]
graphene/PANI	1 mol/L H_2SO_4	0.5 A/g	238 F/g	–	–	[126]
Fe_2O_3/graphene/Ag	LiCl/PVA	2 mA/cm^2	412.3 mF/cm^2	65.4 μWh/cm^2	1.07 mW/cm^2	[125]
NiCoP/MXene	2 mol/L KOH	10 mA/cm^2	20 F/cm^2	0.89 mWh/cm^2	–	[132]
TRGO	1 mol/L H_2SO_4	–	700 mF/cm^2	–	–	[130]
MXene-AgNW-MnONW-C60	PVA-KOH	10 mV/s	216.2 mF/cm^2	19.2 μWh/cm^2	58.3 mW/cm^2	[121]

CD: Current density; ED: Energy density; PD: Power density; SC: Specific capacitance; SS: Scan speed.

allowing operation at low temperatures. The application of 3D printing is a feasible manufacturing means for the construction of flexible supercapacitor devices and the feasible design and manufacture of miniaturized energy storage elements in the device architecture. However, MSCs still face some challenges in providing or collecting energy with a high power and energy capacity.

3.2. Batteries

3D printing can directly use viscoelastic ink with continuous filamentous materials under environmental conditions [142,143]. It is an attractive method for the manufacture and customization of energy storage devices. Zhang *et al.* [72] focused on the energy storage architecture of the electrode through 3D printing. 3D-printed quantum dot microelectronics have very good electronic and ion dynamics. They have an ultra-high specific capacity, high area capacity, and good amplification performance (6 layers, 5.0 mAh/cm^2). Their energy storage capacity is three times that of ordinary lithium storage microelectrodes. They can be directly used as lithium storage anodes. Yee *et al.* [116] integrated an independent, binder-free, conductive, and additive-free LCO structure into LIBs as a cathode. After 100 cycles at C/10, the electrochemical capacity retention was 76%. This simple method of making a 3D LCO structure can be extended to other materials. By customizing the characteristics and chemometrics of a metal salt solution, a general method for the preparation of multicomponent metal oxides with a complex 3D structure is provided. Moreover, Shen *et al.* [144] realized a dendritic-free lithium anode by 3D printing an MXene array, which can guide lithium nucleation and uniformly disperse lithium-ion flux and the electric field. The above characteristics enable the electrode to exhibit a very low potential and good long-period stability.

Lithium sulfur batteries (LSB) are considered to be the next generation of advanced energy storage systems in the future. Wei *et al.* [145] proved that *in situ* oxide implantation can promote the reaction kinetics of polysulfide conversion and explained that the application of 3D printing is conducive to the improvement of sulfur redox kinetics and the ion diffusion coefficient and reduction of the impact of volume change on discharging/charging. Cai *et al.* [104] proposed an innovative idea, designing a V_8C_7-VO_2 heterostructure scaffold based on extrusion 3DP technology. As a dual effective polysulfide fixer and lithium dendrite inhibitor for high-performance LSB, it can effectively adjust polysulfide compounds to reduce their shuttling. The device has an excellent rate performance (643.5 mAh/g at 6.0 C) and cycle stability (capacity attenuation of 0.061% per cycle after 900 cycles at 4.0 C) when applied to an LSB. Shen *et al.* [128] carefully designed a sulfur copolymer graphene structure with a periodic microcrystalline lattice as the cathode of an LSB. The D-type sulfur copolymer graphene system has a high reversible capacity (812.8 mAh/g) and good cycle performance.

Superoxide sodium oxygen batteries (SSOB) are considered to be one of the most promising candidates for next-generation energy storage systems, with a high theoretical energy efficiency and energy density. However, they face problems of low utilization and poor cycle stability. Lin *et al.* [146] produced an rGO air electrode with a hierarchical porous structure by 3D printing. Its electrodes have good O_2/Na^+ transport capacity and good conductivity, which is instrumental for the development of a high-performance Na-O_2 battery. Kong *et al.* [124] adopted a simple and scalable 3D-printing method. 3D printing of quasi-solid state nickel iron battery (QSS-NFB) devices with excellent compressibility, ultra-high energy density (28.1 mWh/cm^3), and excellent long-term cycle durability (more than 1500 cycles even under severe mechanical stress, stable performance) was performed. Shen *et al.* [120] used 3D printing to select KB, a low-cost commercial conductive material with abundant pores, as the main material of selenium sulfide. The reaction kinetics and electrochemical performance of the 3D-printed KB/SeS_2 electrode (3D PKB/SeS_2) under high-quality loading are better than those of an electrode prepared by a traditional roll coating process. The 4-layer printed 3D PKB/SeS_2 honeycomb cathode has a high initial discharge capacity and good cycle stability.

To summarize, 3D printing has been widely used in battery research fields such as lithium ion and lithium sulfur batteries and solid fuel cells. In contrast, vanadium pentoxide as a cathode material has a high theoretical capacitance (2120 F/g) [147], the theoretical capacitance of manganese oxide is up to 386 F/g at a current density of 1 A/g, [148] the theoretical capacitance of graphene is ∼ 550 F/g, [149] the capacitance of multi wall CNTs [150] is up to 135 F/g, and the capacitance of single wall CNTs [151] is up to 180 F/g. In order to maximize the adhesion and mechanical stability between the electrode material and the elastic substrate, a thinner electrode is usually required. However, due to the thin electrode, small electrode volume and insufficient interface area for energy storage, the regional electrochemical performance is inevitably not

Table 2
Application of 3D printing materials in batteries.

Types	Material	CD	Capability	SL	Ref.
LIBs	graphene/poly(lactic) acid	40 mA/g	500 mAh/g	–	[142]
	SnO_2 QDs	0.05 A/g	991.6 mAh/g	–	[72]
	Ag nanoparticle	0.1 C	95 mAh/g	–	[119]
	$LiMn_2O_4$	0.5 C	40 mAh/g	–	[143]
	lithium cobalt oxide	C/40	121 mAh/g	–	[116]
LSBs	3DP-V_8C_7–VO_2/S	6.0 C	643.5 mAh/g	9.2 mg/cm^2	[104]
	3DP-*p*SG	50 mA/g	812.8 mAh/g	–	[128]
	S/BP-2000	10 mA/cm^2	530 mAh/g	2 and 6 mg/cm^2	[152]
Li-SeS_2 batteries	KB/SeS_2	1.8 mA/cm^2	9.5 mAh/cm^2	–	[120]
QSS-NFB	$Ni(OH)_2$ nanosheet	10 mA/cm^2	206.4 mAh/g	–	[124]

CD: Current density; SL: Sulfur Loading.

Table 3
Application of 3D printing materials in electrocatalysis.

Materials	Testing condition	E_j = 10 (V)[b]	Tafel slope (mV/dec)	Ref.
ZIF-67/Ti-E	1.0 mol/L NaOH	360 mV	66	[113]
Gr/AME-Ni Fe10%	0.1 mol/L KOH	519 mV	46	[115]
MoS_x	0.5 mol/L H_2SO_4	−0.297 ± 0.016 V	−119	[156]

Eonset for onset potential (V *vs.* RHE).
E_j = 10 for overpotential required for the current density of 10 mA/cm^2 (V *vs.* RHE).

ideal [152]. The electrochemical energy storage capacity of printable active materials is low, and the construction of electrochemical devices with high electrochemical capacity is still a challenge (Table 2).

3.3. Electro-catalysis

3D printing has the advantages of rapid prototyping and decentralized manufacturing. The 3D framework of 3D printing can provide more electrochemical active sites for electrocatalysis to effectively improve the efficiency of electrochemical energy conversion [153]. Therefore, the application of 3D printing in the field of electrocatalysis is an attractive option. Ying *et al.* [113] designed a 3D-printed titanium electrode (ZIF-67/Ti-E electrode) with a high specific surface area for the electrochemical conversion of ZIF-67 to porous metal oxides for an efficient OER electrocatalyst. In an alkaline medium, the optimized 3D-printed electrode can be directly used as an OER electrode with an excellent electrocatalytic performance. Additionally, Sullivan *et al.* [154] studied the hydrogen evolution reaction (HER) of a 3D-printed porous NiMo-based electrode in 1.0 mol/L KOH solution in an electrochemical H-cell. For comparison, the current density voltage characteristics of the same electrode under a traditional electrode configuration and a flow electrode configuration are studied. It was found that effective hydrogen bubble removal on the electrode surface reduces the losses related to dynamic overpotential and ohmic resistance compared with the traditional planar electrode structure. 3D printing provides unlimited opportunities for the customization of actual substrates or electrodes for various functions. Ng *et al.* [155] synthesized a ReS_2 electrocatalyst on 3D- and 2D-printed electrodes by a simple electrodeposition method. Compared with a blank electrode, the electrocatalytic activity of the HER was significantly improved.

In conclusion, 3D printing has rapidly developed in electrocatalysis (Table 3). Its advantages are summarized as follows: the printing of a 3D structure can provide porous structure to an electrode, effectively improving electron transfer and electrochemical active sites in the process of an electrochemical reaction; furthermore, the application of 3D printing makes it possible to create any independent electrode. For example, the room temperature electrodeposition method allows for coating on 3D electrodes, opening a new method of photo- and electrochemistry [156].

4. Conclusion and outlook

Although materials with various morphologies have been applied to printable inks with certain rheological and mechanical properties, electrode structure design, material selection, and overall device performance play an important role in the application of 3D printing in energy conversion and storage. Herein, we discuss the application of different morphology materials in 3D printing and related synthesis methods.

Functional ink materials with a high viscosity and appropriate rheological properties are the key to realizing rapid and accurate printing. To meet the appropriate 3D-printing requirements, a large number of polymer additives and some thickeners need to be mixed with functional fillers. On this basis, the application of 3D printing in electrochemical fields such as supercapacitors, batteries, and electrocatalysis is discussed. In short, although some achievements have been made in 3D printing, there are still some challenges.

First, the existence of polymer binders and thickeners will affect the electrochemical performance of electrochemical devices. In this process, electrodes are washed repeatedly or annealed at a high temperature. However, this complex operation further reduces the mechanical properties of printed electrodes, destroying the electrode's structure to a certain extent. In order to solve the above problems, on the one hand, the frame structure can not be damaged after annealing by selecting appropriate polymers. On the other hand, some additives (such as fibers, nanowires) can be added appropriately.

Second, there are fewer types of functional nanofillers for limited 3D printing. Although some metal nanowires and nanotubes are considered to be suitable materials, there are relatively few research reports on them. Therefore, the further discovery of new functional filling materials only focuses on the importance.

Third, although a multi-scale pore structure effectively promotes the diffusion and transfer of ions, significantly shortens the diffusion path of ions during charging, and provides active sites for higher electrochemical reactions, there are still some limitations to the fineness and structure of a 3D-printed electrode. In order to solve above problems, a finer printing device can be used, and appropriate additives can be further added to make the printing progress approving.

Fourth, safety is also a challenge in electrochemical applications. Electrolyte decomposition, electrode aging, and overheating will occur in the process of rapid charge and discharge, resulting in potential safety hazards. Therefore, it is very important to find an efficient, simple, and reliable solution for the development of safe electrochemical reaction devices.

Although many materials and structures of 3D-printed electrodes and their required electrolytes have been developed and designed, current research still cannot meet the needs of today's rapidly developing society. Therefore, in the future, research on 3D printing can focus on the design and development of electrode materials and electrode structures, as well as the development and improvement of packaging integration technology in the process of electrochemical testing. On the one hand, new green electrode materials that can be used for 3D printing can be studied, and the diversity and versatility of electrode materials can be further improved to some extent by developing 3D-printing slurries and inks composed of a mixture of various active materials. On the other hand, the design is more conducive to a variety of electrode structures required for 3D printing. In addition, the designed structure can be manufactured using high-precision 3D printing. Subsequently, the required active materials can be deposited on the electrode surface by deposition techniques such as electrochemistry and atomic layer deposition. At the same time, the application of different materials in different fields can be met by improving printing accuracy and using high-precision electrodes and electrolytes. In short, this review has a certain guiding significance for the development and application of 3D-printing materials.

Declaration of competing interest

The authors declare that they have no known competing financial interests or personal relationships that could have appeared to influence the work reported in this paper.

Acknowledgments

This work was supported by the National Natural Science Foundation of China (No. U1904215), Natural Science Foundation of Jiangsu Province (No. BK20200044), Changjiang Scholars Program of the Ministry of Education (No. Q2018270).

References

[1] R. Zhu, J. Ding, L. Jin, H. Pang, Coord. Chem. Rev. 389 (2019) 119–140.
[2] P. Chang, H. Mei, S. Zhou, K.G. Dassios, L. Cheng, J. Mater. Chem. A 7 (2019) 4230–4258.
[3] K. Li, M. Liang, H. Wang, et al., Adv. Funct. Mater. 30 (2020) 2000842.
[4] J. Wang, N. Li, Y.X. Xu, H. Pang, Chem. Eur. J. 26 (2020) 6402–6422.
[5] J. Gu, Y. Xu, Q. Li, H. Pang, Chin. Chem. Lett. 32 (2021) 2017–2020.
[6] J. Liu, H. Wang, R. Ye, P. Jian, L. Wang, J. Colloid Interface Sci. 585 (2021) 61–71.
[7] Z.E. Shi, S.H. Liu, C.H. Tsai, et al., FlatChem 28 (2021) 100254.
[8] A. Qian, Y. Pang, G. Wang, et al., ACS Appl. Mater. Interfaces 12 (2020) 54791–54797.
[9] Q. Li, Z. Shao, T. Han, M. Zheng, H. Pang, ACS Sustain. Chem. Eng. 7 (2019) 8986–8992.
[10] H. Zhou, M. Zheng, H. Tang, et al., Small 16 (2019) 1904252.
[11] B. Li, H. Xue, H. Pang, Q. Xu, Sci. China Chem. 63 (2020) 475–482.
[12] Y. Pang, Y. Cao, Y. Chu, et al., Adv. Funct. Mater. 30 (2019) 1906244.
[13] D.P. Rocha, P.R. Oliveira, B.C. Janegitz, et al., Anal. Chim. Acta 1118 (2020) 73–91.
[14] Z.H. Jaffari, S.M.A. Abuabdou, D.Q. Ng, M.J.K. Bashir, FlatChem 28 (2021) 100256.
[15] W. Zheng, L.Y.S. Lee, ACS Energy Lett. 6 (2021) 2838–2843.
[16] S. Zheng, Y. Zheng, H. Xue, H. Pang, Chem. Eng. J. 395 (2020) 125166.
[17] Y. Bräuniger, S. Lochmann, J. Grothe, M. Hantusch, S. Kaskel, ACS Appl. Energy Mater. 4 (2021) 1560–1567.
[18] C. Wang, X. Li, Q. Li, H. Pang, FlatChem 16 (2019) 100107.
[19] M. Du, Q. Li, Y. Zhao, C. Liu, H. Pang, Coord. Chem. Rev. 416 (2020) 213341.
[20] H. Duan, Z. Zhao, J. Lu, et al., ACS Appl. Mater. Interfaces 13 (2021) 33083–33090.
[21] R. Zhu, J. Ding, J. Yang, et al., ACS Appl. Mater. Interfaces 12 (2020) 25037–25041.
[22] X. Meng, X. Xiao, H. Pang, Front. Chem. 8 (2020) 330.
[23] S. Zheng, X. Guo, H. Xue, et al., Chem. Commun. 55 (2019) 10904–10907.
[24] X. Li, P. Zhu, C. Liu, H. Pang, Chem. Commun. 55 (2019) 9160–9163.
[25] H.V. Doan, H.A. Hamzah, P.K. Prabhakaran, C. Petrillo, V.P. Ting, Nano-Micro Lett. 11 (2019) 54.
[26] S. Hwa Park, H. Jun Park, S. Gyu Son, et al., FlatChem 29 (2021) 100268.
[27] G. Bhattacharya, S.J. Fishlock, A. Pritam, S. Sinha Roy, J.A. McLaughlin, Adv. Sustain. Syst. 4 (2020) 1900133.
[28] A. Ambrosi, R.R.S. Shi, R.D. Webster, J. Mater. Chem. A 8 (2020) 21902–21929.
[29] X. Xiao, L. Zou, H. Pang, Q. Xu, Chem. Soc. Rev. 49 (2020) 301–331.
[30] J. Li, X. Song, W. Zhang, et al., Chem. Eur. J. 26 (2020) 3326–3334.
[31] Z. Hallaji, Z. Bagheri, S.O. Kalji, E. Ermis, B. Ranjbar, FlatChem 29 (2021) 100271.
[32] S. Zhang, Y. Liu, J. Hao, et al., Adv. Funct. Mater. 31 (2021) 2103092.
[33] C. Zhang, M.P. Kremer, A. Seral-Ascaso, et al., Adv. Funct. Mater. 28 (2018) 1705506.
[34] J. Ma, X. Guo, H. Xue, et al., Chem. Eng. J. 380 (2020) 122428.
[35] K. Iwase, S. Stauss, Y. Gambe, R. Miyazaki, I. Honma, ACS Appl. Energy Mater. 4 (2021) 3651–3659.
[36] X. Li, X. Xiao, Q. Li, et al., Inorg. Chem. Front. 5 (2018) 11–28.
[37] L. Zeng, P. Li, Y. Yao, et al., Mater. Today Nano 12 (2020) 100094.
[38] C. Wang, J. Li, Z. Zhou, et al., EnergyChem 3 (2021) 100055.
[39] N. Maldonado, P. Amo-Ochoa, Chem. Eur. J. 27 (2021) 2887–2907.
[40] C. Sun, S. Liu, X. Shi, et al., Chem. Eng. J. 381 (2020) 122641.
[41] A. Akbari, P. Sheath, S.T. Martin, et al., Nat. Commun. 7 (2016) 10891.
[42] Y. Ru, S. Zheng, H. Xue, H. Pang, Chem. Eng. J. 382 (2020) 122853.
[43] L. Chen, X. Guo, W. Lu, et al., Coord. Chem. Rev. 368 (2018) 13–34.
[44] C. Yu, J. An, Q. Chen, et al., Small Methods 4 (2020) 1900824.
[45] Z. Li, Z. Bai, H. Mi, et al., ACS Sustain. Chem. Eng. 7 (2019) 13127–13135.
[46] B. Jiang, Y. Wei, J. Wu, et al., EnergyChem 3 (2021) 100058.
[47] Y. Liu, J. Wang, I. Imaz, D. Maspoch, J. Am. Chem. Soc. 143 (2021) 12943–12947.
[48] S. Yang, Y. Cheng, X. Xiao, H. Pang, Chem. Eng. J. 384 (2020) 123294.
[49] L. Jin, H. Pang, Chin. Chem. Lett. 31 (2020) 2300–2304.
[50] F. Song, G. Li, Y. Zhu, et al., J. Mater. Chem. A 8 (2020) 18538–18559.
[51] P. Yang, H.J. F.an, Adv. Mater. Technol. 5 (2020) 2000217.
[52] R. Zhou, X. Li, H. Pang, Chem. Eng. J. 404 (2021) 126310.
[53] Q.Y. Li, L. Zhang, Y.X. Xu, et al., ACS Sustain. Chem. Eng. 7 (2019) 5027–5033.
[54] H. Zhou, M. Zheng, H. Pang, Chem. Eng. J. 416 (2021) 127884.
[55] F. Zhang, M. Wei, V.V. Viswanathan, et al., Nano Energy 40 (2017) 418–431.
[56] T.T. Lv, Y.Y. Liu, H. Wang, et al., Chem. Eng. J. 411 (2021) 128533.
[57] Y. Li, Y. Shan, H. Pang, Chin. Chem. Lett. 31 (2020) 2280–2286.
[58] M. Zhang, H. Mei, P. Chang, L. Cheng, J. Mater. Chem. A 8 (2020) 10670–10694.
[59] Y. Zang, J. Fan, Y. Ju, H.G. Xue, H. Pang, Chem. Eur. J. 24 (2018) 14010–14027.
[60] F.C. Walsh, C.P. de León, Electrochim. Acta 280 (2018) 121–148.
[61] S.H. Park, G. Goodall, W.S. Kim, Mater. Des. 193 (2020) 108797.
[62] X. Guo, N. Li, Y. Cheng, et al., Chem. Eng. J. 411 (2021) 128544.
[63] Y. Liu, C. Gao, Q. Li, H. Pang, Chem. Eur. J. 25 (2019) 2141–2160.
[64] V. Egorov, U. Gulzar, Y. Zhang, S. Breen, C. O'Dwyer, Adv. Mater. 32 (2020) 2000556.
[65] S. Zheng, H. Xue, H. Pang, Coord. Chem. Rev. 373 (2018) 2–21.
[66] B. Zhang, T. Li, L. Huang, et al., Nanoscale 13 (2021) 5400–5409.
[67] X. Tian, J. Jin, S. Yuan, et al., Adv. Energy Mater. 7 (2017) 1700127.
[68] J. Zhao, H. Lu, X. Zhao, et al., ACS Mater. Lett. 2 (2020) 1041–1056.
[69] X. Qin, B. Yan, J. Yu, et al., Inorg. Chem. Front. 4 (2017) 1424–1444.
[70] Q. Li, X. Li, J. Gu, et al., Nano Res. 14 (2021) 1405–1412.
[71] G. Ge, Y.Z. Zhang, W. Zhang, et al., ACS Nano 15 (2021) 2698–2706.
[72] C. Zhang, K. Shen, B. Li, S. Li, S. Yang, J. Mater. Chem. A 6 (2018) 19960–19966.
[73] Y. Tong, H. Mao, Y. Xu, J. Liu, Inorg. Chem. Front. 6 (2019) 2055–2060.
[74] Y. Liang, Y. Duan, C. Fan, et al., Chem. Eng. J. 360 (2019) 671–679.
[75] Q. Yang, Q. Wang, Y. Long, et al., Adv. Energy Mater. 10 (2020) 1903193.
[76] H. Wang, K. Xie, Y. You, et al., Adv. Energy Mater. 9 (2019) 1901806.
[77] Z. Sun, J. He, M. Yuan, et al., Nano Energy 65 (2019) 103996.
[78] W. Chen, X. Zhang, Y. Peng, et al., J. Power Sources 438 (2019) 227004.
[79] W. Chen, X. Zhang, L.E. Mo, et al., Chem. Eng. J. 375 (2019) 121981.
[80] H. Wu, Q. Yu, C.Y. Lao, et al., Energy Storage Mater 18 (2019) 43–50.
[81] J. Yuan, X. Hu, J. Chen, et al., J. Mater. Chem. A 7 (2019) 9289–9296.
[82] Z. Jin, C. Liu, Z. Liu, et al., Adv. Energy Mater. 10 (2020) 2000797.
[83] X. Wang, Y. Li, S. Wang, et al., Adv. Energy Mater. 10 (2020) 2000081.
[84] J. Zhao, H. Lu, Y. Zhang, et al., Sci. Adv. 7 (2021) eabd6978.
[85] W. Yu, H. Zhou, B.Q. Li, S. Ding, ACS Appl. Mater. Interfaces 9 (2017) 4597–4604.
[86] R. André, F. Natálio, M. Humanes, et al., Adv. Funct. Mater. 21 (2011) 501–509.
[87] Z. Chen, Y. Qin, D. Weng, et al., Adv. Funct. Mater. 19 (2009) 3420–3426.
[88] Z. Chen, V. Augustyn, J. Wen, et al., Adv. Mater. 23 (2011) 791–795.
[89] L. Yin, B. Hu, L. Zhuang, et al., Chem. Eng. J. 381 (2020) 122744.
[90] Y. Wan, P. Qi, D. Zhang, J. Wu, Y. Wang, Biosens. Bioelectron. 33 (2012) 69–74.
[91] W. Xiang, Y. Zhao, Z. Jiang, et al., J. Mater. Chem. A 6 (2018) 23366–23377.
[92] T. Nathan-Walleser, I.M. Lazar, M. Fabritius, et al., Adv. Funct. Mater. 24 (2014) 4706–4716.
[93] C. Zhu, T. Liu, F. Qian, et al., Nano Lett. 16 (2016) 3448–3456.
[94] Y. Jiang, Z. Xu, T. Huang, et al., Adv. Funct. Mater. 28 (2018) 1707024.
[95] B. Yao, S. Chandrasekaran, H. Zhang, et al., Adv. Mater. 32 (2020) 1906652.

[96] Z. Qi, J. Ye, W. Chen, et al., Adv. Mater. Technol. 3 (2018) 1800053.
[97] J. Zhao, Y. Zhang, X. Zhao, et al., Adv. Funct. Mater. 29 (2019) 1900809.
[98] W. Yang, J. Yang, J.J. Byun, et al., Adv. Mater. 31 (2019) 1902725.
[99] J. Orangi, F. Hamade, V.A. Davis, M. Beidaghi, ACS Nano 14 (2020) 640–650.
[100] Z. Fan, J. Jin, C. Li, et al., ACS Nano 15 (2021) 3098–3107.
[101] L. Yu, Z. Fan, Y. Shao, et al., Adv. Energy Mater. 9 (2019) 1901839.
[102] J.D. Cain, A. Azizi, K. Maleski, et al., ACS Nano 13 (2019) 12385–12392.
[103] K. Shen, J. Ding, S. Yang, Adv. Energy Mater. 8 (2018) 1800408.
[104] J. Cai, J. Jin, Z. Fan, et al., Adv. Mater. 32 (2020) 2005967.
[105] Z. Peng, J. Huang, Q. He, L. Tan, Y. Chen, J. Mater. Chem. A 9 (2021) 4273–4280.
[106] T. Wang, L. Li, X. Tian, et al., Electrochim. Acta 319 (2019) 245–252.
[107] W. Wang, Y. Zhang, L. Zhang, et al., Mater. Lett. 213 (2018) 100–103.
[108] B. Yao, S. Chandrasekaran, J. Zhang, et al., Joule 3 (2019) 459–470.
[109] T. Liu, Y. Chen, L. Chen, Acta Metall. Sin. (English Lett.) 34 (2021) 85–97.
[110] M. Kalaj, K.C. Bentz, S. Ayala, et al., Chem. Rev. 120 (2020) 8267–8302.
[111] S. Lawson, A.A. Alwakwak, A.A. Rownaghi, F. Rezaei, ACS Appl. Mater. Interfaces 12 (2020) 56108–56117.
[112] L. Zhong, J. Chen, Z. Ma, et al., Nanoscale 12 (2020) 24437–24449.
[113] Y. Ying, M.P. Browne, M. Pumera, Sustain. Energy Fuels 4 (2020) 3732–3738.
[114] K. Ghosh, S. Ng, C. Iffelsberger, M. Pumera, Chem. Eur. J. 26 (2020) 15746–15753.
[115] P. dos Santos, S.J. Rowley-Neale, A.G.M. Ferrari, J.A. Bonacin, C.E. Banks, ChemElectroChem 6 (2019) 5633–5641.
[116] D.W. Yee, M.A. Citrin, Z.W. Taylor, et al., Adv. Mater. Technol. 6 (2021) 2000791.
[117] X. Tian, K. Tang, H. Jin, et al., Carbon 155 (2019) 562–569.
[118] H.A. Figueredo-Rodríguez, R.D. McKerracher, M. Insausti, et al., J. Electrochem. Soc. 164 (2017) A1148.
[119] M.S. Saleh, J. Li, J. Park, R. Panat, Addit. Manuf. 23 (2018) 70–78.
[120] C. Shen, T. Wang, X. Xu, X. Tian, Electrochim. Acta 349 (2020) 136331.
[121] X. Li, H. Li, X. Fan, X. Shi, J. Liang, Adv. Energy Mater. 10 (2020) 1903794.
[122] T. Wang, X. Tian, L. Li, et al., J. Mater. Chem. A 8 (2020) 1749–1756.
[123] Y. Zhang, T. Ji, S. Hou, et al., J. Power Sources 403 (2018) 109–117.
[124] D. Kong, Y. Wang, S. Huang, et al., ACS Nano 14 (2020) 9675–9686.
[125] K. Tang, H. Ma, Y. Tian, et al., Virtual Phys. Prototyp. 15 (2020) 511–519.
[126] F. Zhou, S. Han, Q. Qian, Y. Zhu, Chem. Phys. Lett. 728 (2019) 6–13.
[127] T. Gao, Z. Zhou, J. Yu, et al., Adv. Energy Mater. 9 (2019) 1802578.
[128] K. Shen, H. Mei, B. Li, J. Ding, S. Yang, Adv. Energy Mater. 8 (2018) 1701527.
[129] X. Tang, C. Zhu, D. Cheng, et al., Adv. Funct. Mater. 28 (2018) 1805057.
[130] A. Azhari, E. Marzbanrad, D. Yilman, E. Toyserkani, M.A. Pope, Carbon 119 (2017) 257–266.
[131] V.G. Rocha, E. García-Tuñón, C. Botas, et al., ACS Appl. Mater. Interfaces 9 (2017) 37136–37145.
[132] L. Yu, W. Li, C. Wei, et al., Nano-Micro Lett. 12 (2020) 143.
[133] S. Ma, Y. Shi, Y. Zhang, et al., ACS Appl. Mater. Interfaces 11 (2019) 29960–29969.
[134] Y. Shao, J.H. Fu, Z. Cao, et al., ACS Nano 14 (2020) 7308–7318.
[135] Y. Chao, Y. Ge, Z. Chen, et al., ACS Appl. Mater. Interfaces 13 (2021) 7285–7296.
[136] B. Yao, H. Peng, H. Zhang, et al., Nano Lett. 21 (2021) 3731–3737.
[137] W. Kang, L. Zeng, S. Ling, R. Yuan, C. Zhang, Energy Storage Mater. 35 (2021) 345–352.
[138] H. Xiao, Z. Wu, L. Chen, et al., ACS Nano 11 (2017) 7284–7292.
[139] S. Liu, X. Shi, X. Li, et al., Nanoscale 10 (2018) 20096–20107.
[140] J. Zhao, Y. Zhang, Y. Huang, et al., Adv. Sci. 5 (2018) 1801114.
[141] Z. Fan, C. Wei, L. Yu, et al., ACS Nano 14 (2020) 867–876.
[142] C.W. Foster, G. Zou, Y. Jiang, et al., Batter. Supercaps 2 (2019) 448–453.
[143] L. Airoldi, U. Anselmi-Tamburini, B. Vigani, et al., Batter. Supercaps 3 (2020) 1040–1050.
[144] K. Shen, B. Li, S. Yang, Energy Storage Mater. 24 (2020) 670–675.
[145] C. Wei, M. Tian, M. Wang, et al., ACS Nano 14 (2020) 16073–16084.
[146] X. Lin, J. Wang, X. Gao, et al., Chem. Mater. 32 (2020) 3018–3027.
[147] M. Zhi, C. Xiang, J. Li, M. Li, N. Wu, Nanoscale 5 (2013) 72–88.
[148] N. Yu, H. Yin, W. Zhang, et al., Adv. Energy Mater. 6 (2016) 1501458.
[149] G.F. Hawes, S. Rehman, M.A. Pope, Curr. Opin. Electrochem. 20 (2020) 36–45.
[150] C. Du, N. Pan, Nanotechnology 17 (2006) 5314.
[151] D.N. Futaba, K. Hata, T. Yamada, et al., Nat. Mater. 5 (2006) 987–994.
[152] X. Gao, X. Yang, Q. Sun, et al., Energy Storage Mater. 24 (2020) 682–688.
[153] N.A. Kyerematen, T. Brousse, D. Pech, Nat. Nanotechnol. 12 (2017) 7–15.
[154] I. Sullivan, H. Zhang, C. Zhu, et al., ACS Appl. Mater. Interfaces 13 (2021) 20260–20268.
[155] S. Ng, C. Iffelsberger, Z. Sofer, M. Pumera, Adv. Funct. Mater. 30 (2020) 1910193.
[156] C. Iffelsberger, S. Ng, M. Pumera, Appl. Mater. Today 20 (2020) 100654.

Huan Pang received his Ph. D. degree from Nanjing University in 2011. He is now a university distinguished professor at Yangzhou University and Young Changjiang Scholars of the Ministry of Education, China. He is a senior member of the China Chemical Association. He is the managing editor of EnergyChem, the editorial board member of FlatChem and Rare Metals, and the youth editorial board member of e-Science, Advanced Fiber Materials, Chinese Journal of Inorganic Chemistry, and Chinese Chemical Letters. He was recognized as a highly cited researcher in Cross-Field by Clarivate Analytics in 2020.